Eur. Phys. J. D (2025) 79:120
https://doi.org/10.1140/epjd/s10053-025-01068-w

THE EUROPEAN PHYSICAL JOURNAL D

Regular Article - Atoms, Molecules, Ions, and Clusters

Interaction of 25 eV electrons with DNA constituents: XPS analysis of calf thymus DNA, nucleosides, and nucleobases

João Pereira-da-Silva[1], Hao Yu[2,a], Bo-An Chen[2,3], Pitambar Sapkota[2,4], Filipe Ferreira da Silva[1], and Sylwia Ptasińska[2,4]

[1] CEFITEC, Departamento de Física, NOVA School of Science and Technology, Universidade NOVA de Lisboa, 2829-516 Caparica, Portugal
[2] Radiation Laboratory, University of Notre Dame, Notre Dame, IN 46556, USA
[3] Department of Chemistry and Biochemistry, University of Notre Dame, Notre Dame, IN 46556, USA
[4] Department of Physics and Astronomy, University of Notre Dame, Notre Dame, IN 46556, USA

Received 25 June 2025 / Accepted 15 September 2025 / Published online 6 October 2025

Abstract. Understanding the interactions of secondary electrons generated by ionizing radiation provides a fundamental basis for developing strategies in cancer therapy. In this study, we investigated the interactions of 25 eV low-energy electrons (LEEs) with calf thymus DNA and its constituents, four types of nucleosides and nucleobases, using X-ray photoelectron spectroscopy (XPS). Based on the acquisition and analysis of core-level spectra (O 1s, C 1s, N 1s, and P 2p) in DNA, structural changes induced by 25 eV electrons suggest potential site- and base-specific selectivity. These changes may involve hydroxyl (C–OH) group release from the sugar moiety, cleavage of C–N bonds (likely corresponding to N-glycosidic linkages), and phosphate backbone damage in calf thymus DNA. Among the four nucleosides, thymidine and guanosine showed more evident structural modifications, while cytidine and adenosine were relatively stable. In addition, nucleosides displayed greater susceptibility to LEE-induced structural changes than their corresponding nucleobases. This study reveals the selective damage mechanisms of LEEs on various DNA constituents, which may provide mechanistic insights for future developments in precision cancer therapy based on molecular-level damage.

1 Introduction

DNA is composed of two long polynucleotide chains and encodes the genetic information required for the synthesis of proteins and RNA in living organisms [1, 2]. In cells, if severe DNA damage occurs and is not properly repaired, the resulting chromosomal discontinuities often lead to cell death [3]. Types of DNA damage are classified based on the number of lesions and their specific locations within the DNA molecule, such as base release, single-strand breaks (SSBs), double-strand breaks (DSBs), multiple double-strand breaks (MDSBs), and DNA–DNA or DNA–protein crosslinks [4, 5].

As a major contributor to DNA damage and cell death, ionizing radiation has been widely utilized as an effective therapeutic modality in cancer treatment [6]. High-energy ionizing radiation (e.g., γ-rays, X-rays, protons, and heavy ions) releases a substantial amount of energy upon interacting with living cells, which can effectively alter the chemical structure of DNA and lead to mutagenic and cytotoxic effects [7, 8]. Radiation-induced DNA damage is generally categorized as either direct or indirect, depending on whether the ionization occurs within the DNA molecule itself or in the surrounding medium [6, 9, 10]. Direct DNA damage refers to DNA being directly exposed to ionizing radiation and its secondary species, initiating a sequence of damage processes. In contrast, Indirect DNA damage refers to damage caused by radiolytic products generated in the surrounding medium. When water molecules absorb energy from ionizing radiation, they generate highly reactive species, such as hydroxyl radicals (·OH), which can lead to DNA damage [10–12]. The effects of these indirect processes are primarily governed by the lifetimes of the reactive species [13] and the presence of radical scavengers, which modulate their reactivity [14].

As part of the direct action, prehydrated electrons, transient species formed before complete solvation, are considered among the most lethal agents to DNA

Supplementary Information The online version contains supplementary material available at https://doi.org/10.1140/epjd/s10053-025-01068-w.

[a] e-mail: hyu5@nd.edu (corresponding author)

[15]. These electrons are a dominant type of secondary species generated during ionizing radiation, with approximately 5×10^4 ballistic electrons produced per MeV of deposited energy [16, 17]. Specifically, low-energy electrons (LEEs), which are defined as having energies below 100 eV, can induce various types of damage through their direct interactions with DNA [18]. Sanche and coworkers demonstrated that LEEs with energies below the electronic excitation threshold of DNA can induce strand breaks in plasmid DNA [4, 16, 19]. Following these studies, further research revealed that LEEs with energies below 15 eV can initiate strand breaks via the formation of a transient negative ion (TNI) upon electron capture by DNA components, followed by bond dissociation through dissociative electron attachment (DEA) [18, 20]. LEEs in the range of 5–40 eV were found to induce anion desorption through both resonant and nonresonant processes, revealing base-specific sensitivities [20]. Furthermore, in the energy range of 0–19 eV, LEEs have been shown to induce phosphate-related bond scission via DEA [21]. Several studies have also demonstrated that LEEs can induce strand breaks of DNA by cleaving the C–O bond of the phosphodiester linkage between the deoxyribose sugar and the phosphate group [18, 20, 22].

DNA strand breaks induced by LEEs in the energy range of 15–100 eV are primarily attributed not only to multiple electron energy loss events due to scattering, but also to non-resonant mechanisms such as electronic excitation, ionization, and direct dissociation [4]. It has been reported that above the threshold for dipolar dissociation ($\sim$ 15 eV), the yields of SSBs and DSBs increase monotonically, reaching a plateau near 30 eV with an intensity comparable to that observed at 10 eV [20]. The yield of MDSBs exhibits a pronounced monotonic increase in the 30–100 eV energy range, indicating that higher-energy LEEs are more likely to induce DNA clustered strand breaks [4]. Building on these findings, subsequent mass spectrometric studies systematically investigated LEE-induced decomposition of nucleobases and their corresponding nucleosides, including thymine [23], thymidine and uridine [24], purine nucleobases [25], and adenine [26], revealing base–sugar bond cleavage, formation of fragment anions, and specific dissociation pathways under electron impact. However, other analytical methods have been used to gain an understanding of LEE interactions with DNA molecules, especially at the molecular level. Among these, XPS enables the investigation of chemical transformations by revealing both structural modifications and changes in elemental composition of DNA during LEE irradiation. For instance, XPS-based investigations have demonstrated that the presence of a water atmosphere can influence the extent of DNA damage induced by LEEs [15]. Further studies have employed XPS to evaluate the effects of 5 eV LEE irradiation on DNA [27], as well as the synergistic DNA damage resulting from the combined action of Fe^{3+} ions and LEEs [28]. Expanding upon previous research, we performed comprehensive investigations of chemical changes in DNA induced by LEEs at an energy of 25 eV. This energy regime enables not only DEA but also electronic excitation, ionization, and direct dissociation, highlighting the complex interplay of damage pathways. To resolve this complexity, we compared the chemical changes observed in individual DNA constituents with those found in DNA after irradiation, which allowed us to provide deeper insights into LEE-induced mechanisms.

2 Materials and methods

2.1 Chemicals and sample preparation

Calf thymus double-stranded DNA (molecular weight = 1.0–1.5 $\times$ 10^7 Da) in sodium chloride solution, nucleosides (thymidine, adenosine, cytidine, and guanosine), and nucleobases (thymine, adenine, cytosine, and guanine) were purchased from Sigma-Aldrich and used without further purification. Figure S1 summarizes the molecular structures of four nucleosides and their corresponding nucleobases. Aqueous solutions of each compound (1 mg/ml) were drop-cast onto silicon substrates covering an area of 8 mm $\times$ 8 mm, followed by drying under vacuum at room temperature to form a thin solid film. Before DNA sample deposition, the silicon wafers were cleaned with a 1:1 (v/v) mixture of deionized water and ethanol, then immediately immersed in 20 ml of ethanol and sonicated for 30 min. Afterwards, the substrate was dried using compressed air and cleaned with air plasma for 15 min to remove surface organic contaminants.

2.2 LEE irradiation

LEE irradiation experiments were carried out in a high-vacuum chamber with a base pressure below 2×10^{-10} mbar. The prepared DNA samples were exposed to 25 eV electrons. Each DNA sample was subjected to cumulative irradiation through sequential 30-min exposures. Accordingly, the spectra labeled as 60, 90, 120, and 150 min correspond to the same sample after 2, 3, 4, and 5 consecutive 30-min exposures, respectively. The electron beam current was monitored with an ammeter (Keithley Instruments, Cleveland, OH, USA). To minimize charging effects, all samples were placed on grounded sample holders using silver conductive paint. Electrons were thermionically emitted from a tungsten hairpin filament, focused by the electron optics, and subsequently accelerated to 25 eV by a potential difference between the electron gun and ground. The particle fluence F is defined as the ratio of the total number of electrons N_e to the irradiated area A. The number of electrons N_e can be calculated from the irradiation time t and the beam current I measured at the sample (Eq. 1):

$$F = \frac{N_e}{A} = \frac{I \cdot t}{A \cdot e} \quad (1)$$

where e is the elementary charge.

2.3 XPS data acquisition and analysis

Before and after LEE irradiation, thin films of calf thymus DNA, nucleosides, and nucleobases were analyzed using XPS with a SPECS Surface Nano Analysis system (Germany). Details of XPS instrument have been described elsewhere [29]. Briefly, the XPS system is equipped with an anode X-ray source, a hemispherical electron energy analyzer, and a detector consisting of nine microchannel plates. The XPS generates an Al Kα X-ray beam (70 W, photon energy = 1486.6 eV) from an aluminum anode in a microfocus X-ray source equipped with a quartz crystal, which monochromatizes the X-ray beam. The X-ray beam was incident at an angle of approximately 60° relative to the surface normal. Survey spectra were collected with a pass energy of 70 eV and a step size of 1.0 eV, giving a total resolution of ∼ 1.0–1.5 eV. In addition, all high-resolution C 1s, N 1s, and O 1s spectra were acquired with a pass energy of 20 eV and a step size of 0.05 eV, corresponding to a total energy resolution of ˜ 0.6–0.8 eV.The same acquisition parameters were used for all samples, including the calf thymus DNA films, nucleosides, nucleobases, and substrate, allowing all spectra to be directly compared. Each elemental region, including carbon (C 1s), nitrogen (N 1s), and oxygen (O 1s), was typically measured over 30 min. For calf thymus DNA, the total acquisition time was extended to approximately 1 h due to the low intensity of the phosphorus (P 2p) region. Control samples, including the bare silicon substrate and unirradiated DNA, were also scanned five times under the same conditions as the irradiated samples.

All photoelectron spectra were calibrated by referencing the first peak (Peak 1, corresponding to C–C/C–H bonding) in the C 1s region to 285.0 eV. Peak deconvolution was performed for the C 1s, N 1s, O 1s, and P 2p regions using multiple Gaussian components in CasaXPS. Where appropriate, the full width at half maximum (FWHM) of selected peaks was constrained to 1–2 eV. After peak deconvolution, relative peak area ratios (%) were determined from the corresponding peak areas as follows (Eq. 2):

$$\text{Peak ratio (\%)} = \left(\frac{A_i}{A_{\text{total}}}\right) \times 100 \quad (2)$$

where A_i is the area of the individual fitted peak. A_{total} is the total area of all fitted peaks for the corresponding element. The uncertainty in the XPS measurements, arising from factors such as peak fitting, surface conditions variability, and instrumental limitations, is estimated to be around 10–20% [30]. This uncertainty is associated with each data point in the figures, which present the relative peak area ratios as a function of irradiation time. As the error was predominantly systematic and remained consistent across all data points, identical error bars would be applied throughout the dataset. Consequently, the error bars were omitted from these figures. Nonetheless, the uniform uncertainty has been taken into account in the data interpretation and discussion.

3 Results and discussion

3.1 Overview of survey and core-level spectra with peak assignments

Figure 1 presents the full survey spectra of the SiO_2 substrate, calf thymus DNA, and selected nucleosides to confirm the elemental composition of the sample. All subsequent high-resolution spectra were calibrated by referencing the C–C component of the C 1 s peak at 285.0 eV and used for detailed chemical state analysis. For the SiO_2 substrate, only O 1s (∼ 533 eV), Si 2s (∼155 eV), Si 2p (∼ 105 eV), and O 2s (∼ 28 eV) peaks were observed. After deposition of calf thymus DNA, most Si substrate signals were no longer detectable. Instead, peaks corresponding to C 1s (∼ 286 eV), N 1s (∼ 400 eV), O 1s (∼ 533 eV), and P 2p (∼ 135 eV) appeared, together with minor contributions from Na KLL (∼ 496 eV) and Cl 2p (∼ 192 eV). The O 1s, N 1s, C 1s, and P 2p peaks arise from DNA, whereas the Na KLL and Cl 2p peaks are attributed to residual salts. The disappearance of Si peaks indicates that the DNA films completely covered the substrate. The effective thickness of the DNA films, therefore, exceeded the maximum XPS detection depth, estimated at ˜ 10 nm. However, in a few cases (e.g., guanosine and all nucleobase samples; see Supporting Information, Fig. S2), minor Si 2p and Si 2s signals were still detected. This may be attributed either to incomplete coverage of the substrate or to partial signal transmission through thinner regions of the DNA films.

Figure 2 presents the photoelectron spectra of the C 1s, N 1s, O 1s, and P 2p regions of calf thymus DNA following 25 eV LEE irradiation for 30, 60, 90, and 120 min. Unless otherwise stated, data collected at 0 min (before irradiation) were only used as references and are not shown in the figures. This is because samples were prepared outside a high vacuum under ambient conditions and often show instability, which can interfere with signal interpretation. Representative high-resolution spectra before electron irradiation are provided in the Supporting Information (Fig. S3). The O 1s, N 1s, and C 1s peaks of individual nucleosides (Figs. S4, S5, S6 and S7) and their corresponding bases (Figs. S8, S9, S10 and S11) are provided in the Supporting Information to illustrate their spectral similarities and differences. For clarity and consistency, the nucleosides and their corresponding nucleobases are discussed in the order of thymine (T), adenine (A), cytosine (C), and guanine (G) throughout the text. In general, due to the mixed nucleoside composition of calf thymus DNA,

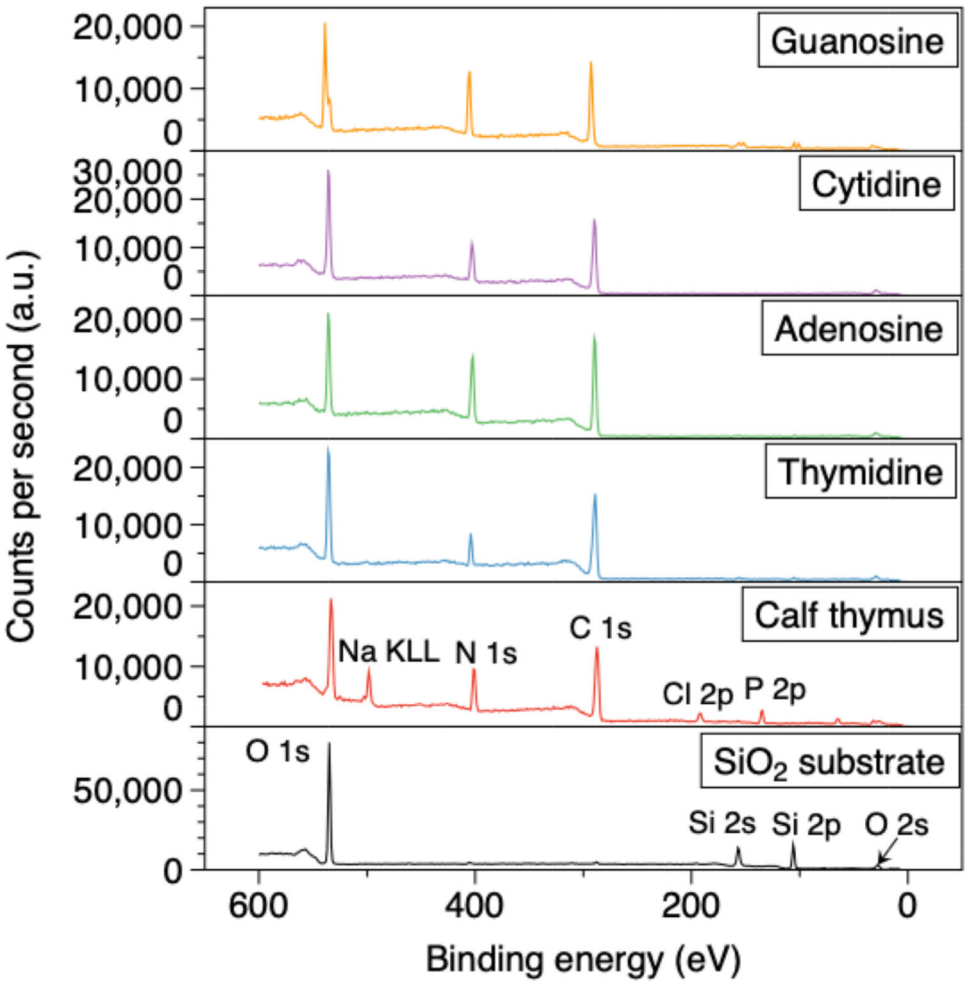

Fig. 1 Survey XPS spectra of the SiO_2 substrate, calf thymus DNA, and nucleosides

the chemical environment is more complex, and the corresponding peaks are therefore typically broader than those of individual nucleosides.

During irradiation, a decrease in the maximum intensity of the peaks was observed. Specifically, the reductions in the C 1s, N 1s, and O 1s signals occurred around 287 eV, 400–401 eV, and 533 eV, respectively, corresponding to the higher binding energy components within each region. This observation remains reasonable even when considering potential peak shifts caused by deconvolution uncertainty. In contrast, the nucleosides and nucleobases exhibited different trends in peak intensity decrease during irradiation. In thymidine, the O 1s and N 1s peaks decreased significantly, and a lower signal was also observed in the higher binding energy region of the C 1s peak (Fig. S4). In adenosine, the O 1s peak showed a pronounced decrease (Fig. S5). Cytidine exhibited a decrease in the O 1s peak (Fig. S6), while guanosine showed decreases in O 1s, N 1s, and C 1s signals (Fig. S7). Among the nucleobases, only cytosine (Fig. S10) and guanine (Fig. S11) displayed similar decreasing trends. These differences may reflect site-selective damage at specific structural constituents such as the base, sugar moiety, or phosphate backbone.

Figure 3 shows the peak fitting of photoelectron spectra for calf thymus DNA after 30 min of electron irradiation. The peak assignments and their corresponding binding energies, referenced from the literature [10, 15, 31], are summarized in Table 1. Owing to slight structural differences among the DNA types, peak fitting procedures were adapted accordingly rather than applied uniformly. Peak 4 is often difficult to classify unambiguously, as it overlaps with peak 3 in the C 1s region. Due to the weak intensity of this component and the close binding energies, clear separation is challenging. Therefore, peak 4 is considered a minor carbonyl-type contribution (e.g., O–C=O, N–C=O environments), distinguishable in nucleosides but not resolved in calf thymus DNA.

3.2 Detachment of C–OH groups revealed by O 1 s and C 1 s spectral features

Figure 4 shows the relative peak area ratios of the C 1s, O 1s, and N 1s peaks for calf thymus DNA and calculated using Eq. 2. To improve visual clarity, error bars corresponding to a 10% uncertainty have been omitted. We did not present results for P 2p, because phosphorus appears as two peaks due to spin–orbit splitting (P

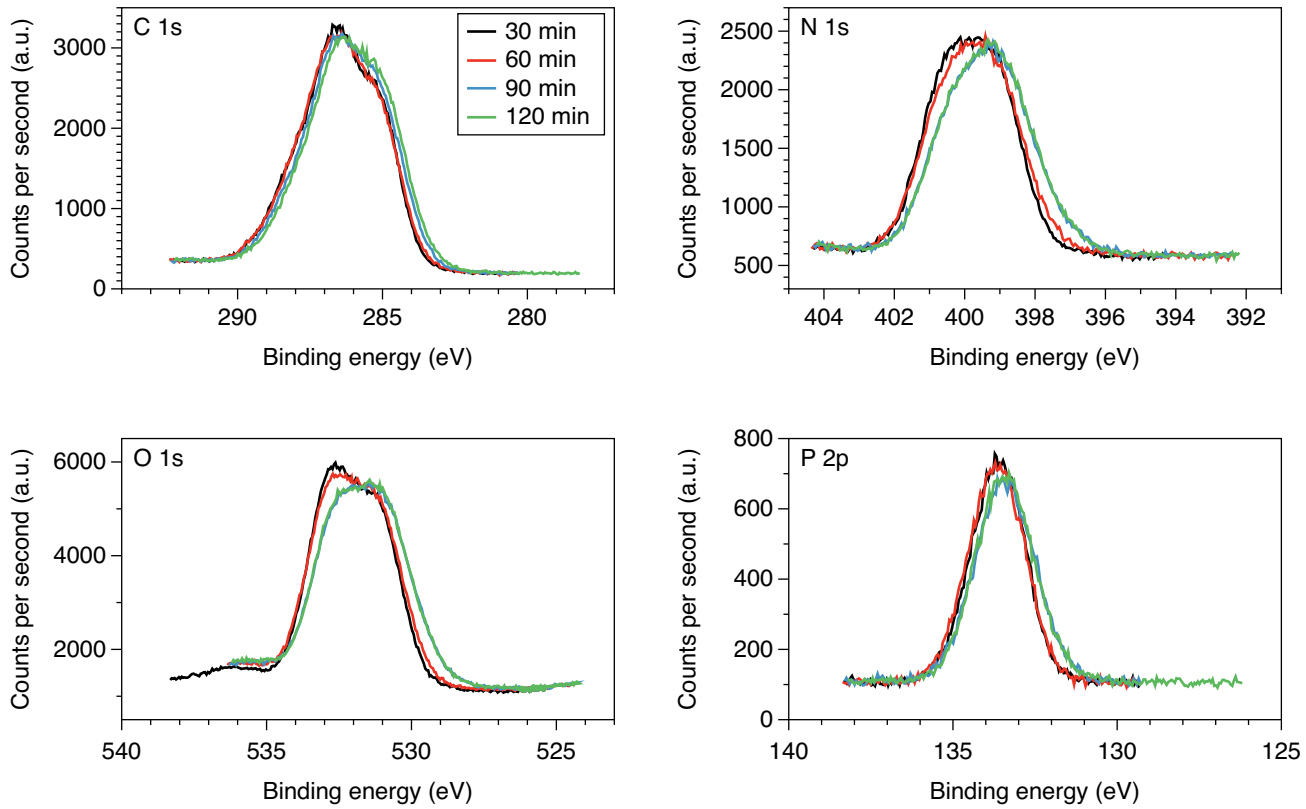

Fig. 2 Photoelectron spectra of the C 1s, N 1s, O 1s, and P 2p regions for calf thymus DNA after 25 eV electron irradiation for 30 (black curve), 60 (red curve), 90 (blue curve), and 120 (green curve) min

$2p_{3/2}$ and P $2p_{1/2}$), and their relative positions remain unchanged under all conditions. In the O 1 s spectrum, the peak area ratio of peak 2 (C–OH) decreased, while that of peak 1 (O in phosphate group, C=O) increased. In the C 1 s spectrum, peak 2 (C–O and C–N) also slightly decreased, as the changes also reflected in the O1s spectrum. These changes are attributed to electron-induced decomposition, likely due to the desorption of small molecular fragments such as OH. Detachment of hydroxyl groups (C–OH) refers to the cleavage of which OH moieties from the parent molecular structure through bond dissociation, resulting in their release as ionic species [32].

Figures 5 and 6 show the changes in the relative O 1 s and C 1 s peak area ratios of four nucleosides under 25 eV LEE irradiation: (a) thymidine, (b) adenosine, (c) cytidine, and (d) guanosine. For adenosine (Fig. 5b), only a single O 1 s component is present, which limits the applicability of peak deconvolution. In the case of guanosine (Fig. 5d), a substrate-related silicon signal interferes with the spectrum, reducing the accuracy of peak area quantification. In addition, the peak fitting varied depending on the structural differences among the nucleosides. Specifically, four peaks were resolved for thymidine (Fig. 6a), cytidine (Fig. 6c), and guanosine (Fig. 6d), whereas only three peaks were detected for adenosine (Fig. 6b).

In thymidine, a decrease in the C–OH signal was observed in both the O 1 s spectrum (Fig. 5a, peak 2) and the C 1 s spectrum (Fig. 6a, peak 2). These changes suggest that the release of the OH group from the sugar ring may be accompanied by the formation and transformation of C–O bonds into other chemical groups. According to previous gas-phase studies [24, 25], the mass spectrum of thymidine exhibits extensive fragmentation and a very low intensity of the parent cation, indicating a structurally fragile molecule. Two of the most abundant fragments are the protonated thymidine and a sugar-ring-associated cation [24]. Moreover, during the sugar ring fragmentation, the most abundant fragment is formed by the removal of an OH radical [24].

In adenosine, the O 1s component corresponding to the C–OH group remained constant (Fig. 5b, peak 2), and no significant change in the relative peak area ratio of this signal was observed in the C 1s spectrum (Fig. 6b, peak 2). However, a gradual decrease in the absolute peak intensities of both O 1s and C 1s was noted (Fig. S5). Considering that the O 1s signal mainly originates from the C–O bonding state in the sugar ring, we speculate that partial cleavage of the OH group may have occurred. However, the limited extent of this release likely accounts for the absence of an apparent change in the C 1s peak ratio.

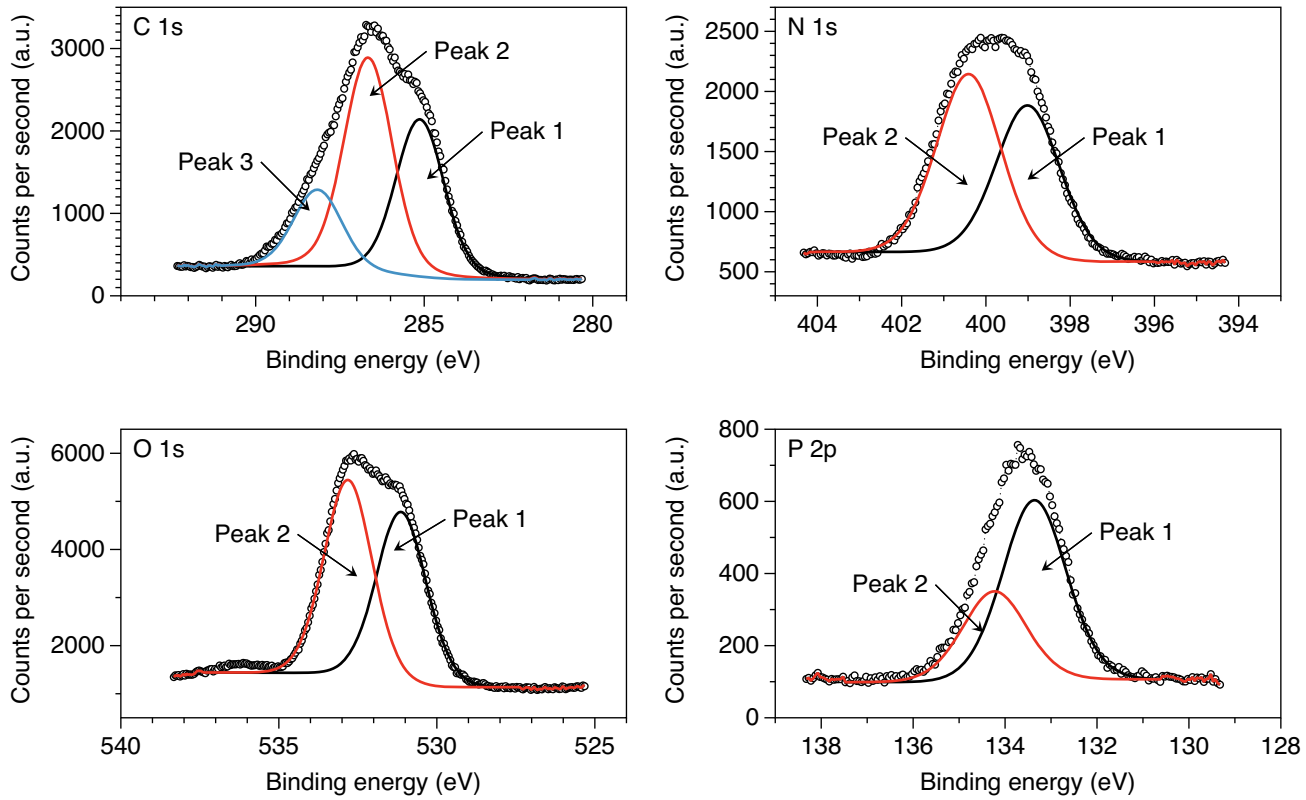

Fig. 3 Peak fitting of the C 1s, N 1s, O 1s, and P 2p photoelectron spectra of calf thymus DNA after 25 eV low-energy electron irradiation for 30 min (representative examples)

In cytidine, a decrease in the C–OH signal was observed in the O 1s spectrum (Fig. 5c, peak 2), accompanied by a slight decrease in the corresponding peak in th C 1s spectrum (Fig. 6c, peak 2). These changes, together with the overall decrease in absolute O 1s intensity (Fig. S6), support the occurrence of C–OH detachment in cytidine.

In guanosine, the relative peak ratio was relatively stable in O 1s and C 1s (peak 2 in Fig. 5d and 6d), but the peak intensity signal was decreased (Fig. S7). The behavior observed in guanosine indicates a distinct chemical change compared to the other nucleosides. Previous studies have shown that localized damage in guanine-containing nucleosides is particularly significant [33, 34]. During ionization, an electron is ejected, and the resulting hole can migrate along the DNA molecule. Guanine is the most easily oxidized of the four canonical bases due to its lowest oxidation potential [35], and its corresponding nucleotide is widely used as a DNA model for studying redox behavior under ionizing conditions [14]. This property makes it the preferred site for hole localization, rendering guanine highly susceptible to subsequent chemical damage under conditions of ionizing or electronic excitation. As a result, damage tends to concentrate at guanine bases [14] and single-strand breaks (SSBs) in the DNA backbone [15].

Previous Electron-Stimulated Desorption (ESD) experiments on DNA have demonstrated that OH^- can be generated during LEE irradiation [18, 20, 36]. Fragments containing O^- and OH^- were detected following electron exposure [18, 20], and O^- may generate OH^- via reactive scattering through the following reaction (Eq. 3) [36]:

Table 1 Binding energies (eV) of elements and their corresponding chemical bond assignments

Element	Peak No	BE (eV)	Peak assignment [10, 15, 31]
C 1s	1	285	C–C, C–H, C=C
C 1s	2	286–287	C–O, C–N
C 1s	3	287–288	C=O, N–C–O
C 1s	4 (optional)	288–289	O–C=O, N–(C=O)–N
N 1s	1	398–400	N=C, –N=
N 1s	2	400–402	C–N, $–NH_2$
O 1s	1	531–532	O in Phosphate group, C=O
O 1s	2	532–533	C–OH, C–O–C
P 2p	1	133	P $2p_{3/2}$
P 2p	2	134	P $2p_{1/2}$

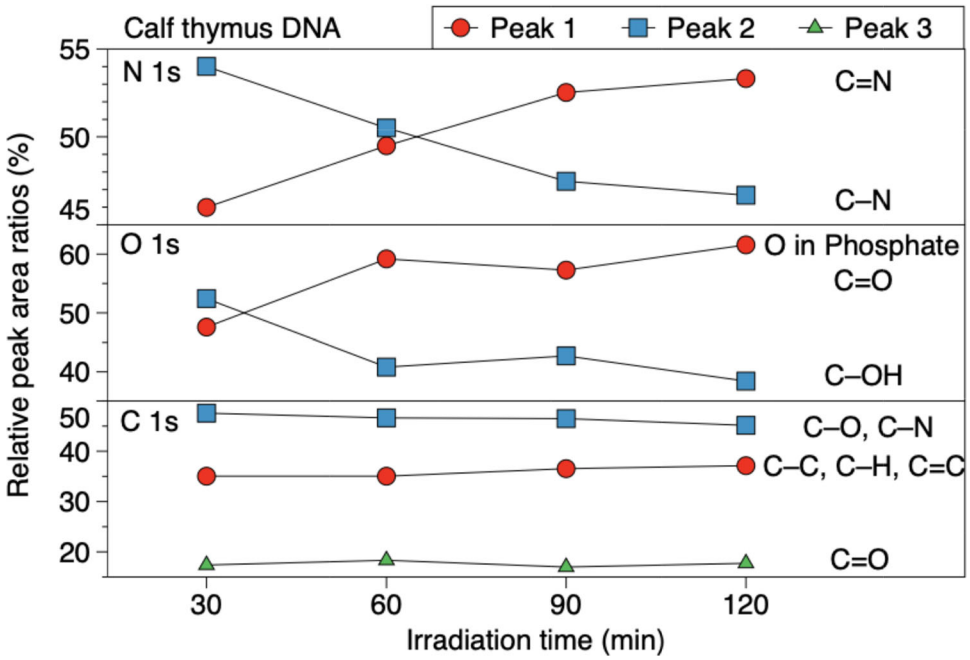

Fig. 4 Relative peak area ratios of C 1s, O 1s, and N 1s peaks for calf thymus DNA

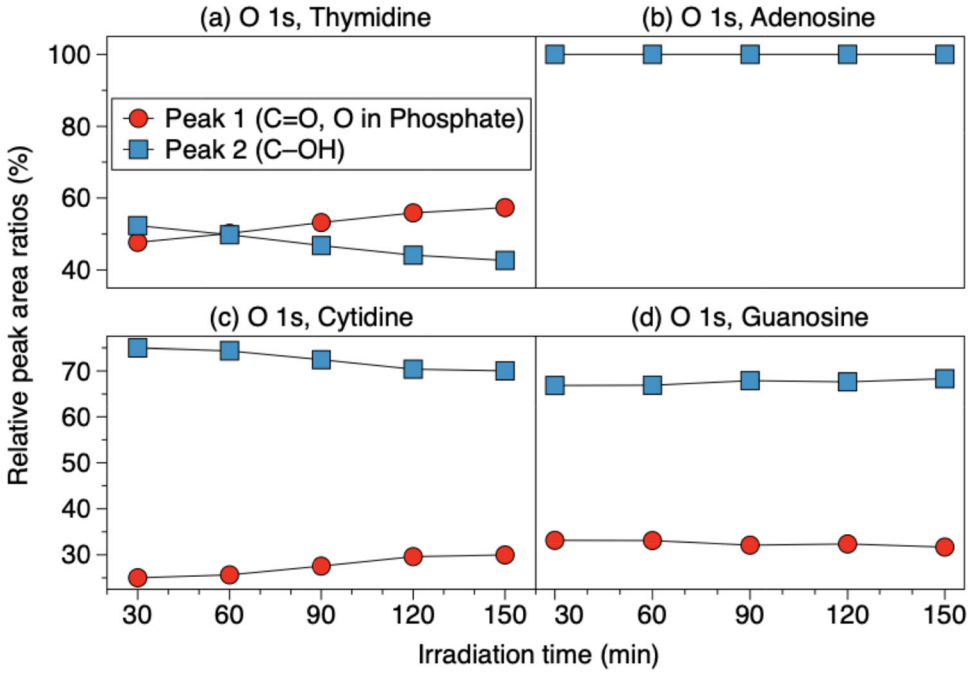

Fig. 5 Relative O 1s peak area ratios of (**a**) thymidine, (**b**) adenosine, (**c**) cytidine, and (**d**) guanosine under 25 eV LEE irradiation for 30, 60, 90, 120, and 150 min

$$O^- + C_xH_{2x+2} \rightarrow (C_xH_{2x+2}O)^{*-} \rightarrow OH^- + C_xH_{2x+1} \quad (3)$$

Interestingly, peak 2 (C–OH) in th O 1s spectra decreased in thymidine (Fig. 5a) and cytidine (Fig. 5c), whereas it remained relatively stable or slightly increased in adenosine (Fig. 5b) and guanosine (Fig. 5d). Given that thymidine and cytidine are pyrimidine nucleosides, while adenosine and guanosine are purines, these differences in spectral behavior may reflect structural variations and distinct damage pathways characteristic of each nucleoside type.

Several additional phenomena were observed. First, peak 3 (C=O) in th C 1s spectra (Fig. 6) of cytidine and guanosine decreased with increasing LEE irradiation time, suggesting that C=O-containing groups may also undergo degradation upon prolonged LEE exposure. At an energy of 25 eV, both DEA and electronic excitation processes can occur, which may contribute to the observed C=O damage.

Furthermore, peak 4 (O–C=O) increased in thymidine, cytidine, and guanosine with longer irradiation times, while it was absent in adenosine. This trend is consistent with the molecular structures, as adenosine

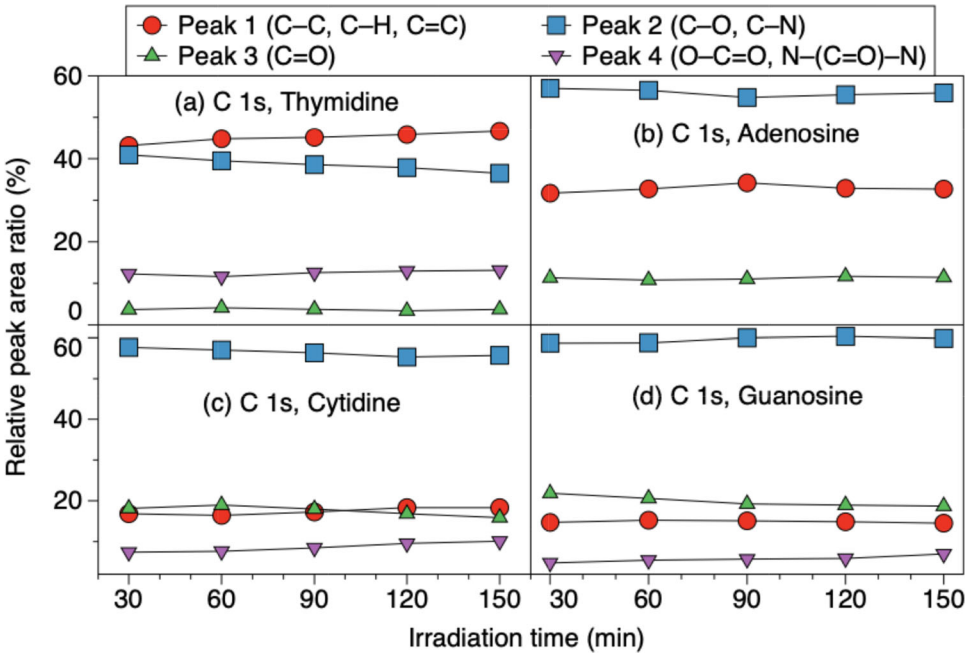

Fig. 6 Relative C 1s peak area ratios of (**a**) thymidine, (**b**) adenosine, (**c**) cytidine, and (**d**) guanosine under 25 eV LEE irradiation for 30, 60, 90, 120, and 150 min

lacks an inherent C=O group. LEE irradiation may promote the formation of O–C=O species in nucleosides containing C=O functionalities. Although the increase in the O–C=O signal supports the occurrence of LEE-induced oxidative processes, similar to the trend observed for peak 3, the influence of uncertainties in peak deconvolution cannot be entirely excluded.

Additionally, for the isolated nucleobases, slight decreases in the O 1s and C 1s signal intensities were observed in cytosine and guanine (Figs. S10 and S11), suggesting that oxygen-related chemical modifications may have partially occurred within the base moieties.

3.3 Nitrogen spectral evidence for C–N cleavage

A decrease in the C–N bonding signal was observed in both the N 1s (peak 2) and C 1s (peak 2) spectra of calf thymus DNA after 25 eV electron irradiation (Fig. 4), consistent with potential cleavage of the C–N bonds. In the DNA structure, C–N bonds are present at two distinct sites: within the nucleobases and at the N-glycosidic bond linking the base to the sugar moiety. Except for guanine (Fig. S11), the N 1s signal intensities of the other three nucleobases did not show significant changes during irradiation, suggesting that cleavage of the N-glycosidic bond may have occurred. The N-glycosidic bond is critical as it connects the nucleobase to the sugar moiety, which in turn links to the phosphate backbone. Cleavage of the N-glycosidic bond can lead to the formation of apurinic/apyrimidinic sites. This is especially relevant biologically, as base excision repair begins by removing damaged or modified bases through N-glycosidic bond hydrolysis, helping maintain genome stability [37].

Figure 7 displays the relative N 1s peak area ratios of four nucleosides under 25 eV LEE irradiation for 30, 60, 90,120 and 150 min: (a) thymidine, (b) adenosine, (c) cytidine, and (d) guanosine. Similar to the results observed for calf thymus DNA, a gradual decrease in the C–N signal was found in thymidine, both in the N 1s spectrum (Fig. 7a, peak 2) and th C 1s spectrum (Fig. 6a, peak 2). Meanwhil peak (C=N) in the N 1 s spectrum showed a gradual increase. As discussed previously, no significant damage was observed in the corresponding nucleobase (thymine, Fig. S8), suggesting that the primary site of damage was likely the N-glycosidic bond. The DEA studies of thymidine suggest that LEEs efficiently decompose this molecule into the sugar and thyminyl moiety associated with the N-glycosidic bond cleavage [23].

In adenosine, no significant spectral changes were observed after irradiation (Fig. S5). However, a slight decrease in the intensity of peak 1 (C–N) was noted in both the C 1s (Fig. 6b) and N 1 s (Fig. 7b) spectra. This observation may suggest a limited cleavage of the N-glycosidic bond and the possible formation of a new bonding configuration, such as a C=N (imine-type) species. Nevertheless, due to the subtle nature of these changes, it is also possible that they result from uncertainties in the peak deconvolution process rather than actual structural transformations.

In cytidine, no significant change was observed in the relative intensity corresponding to the C–N bond in either the C 1 s spectrum (Fig. 6c, peak 2) or the N 1 s spectrum (Fig. 7c, peak 2), indicating that the N-glycosidic bond remained stable under LEE irradiation. Among the four nucleosides, cytidine exhibited the least evidence of C–N bond cleavage.

In guanosine, a decrease in the area of peak 1 (C=N) at low binding energy was observed in the N 1 s spectrum (Fig. S7), and a similar trend was further confirmed in guanine (Fig. S11, N 1 s). These changes

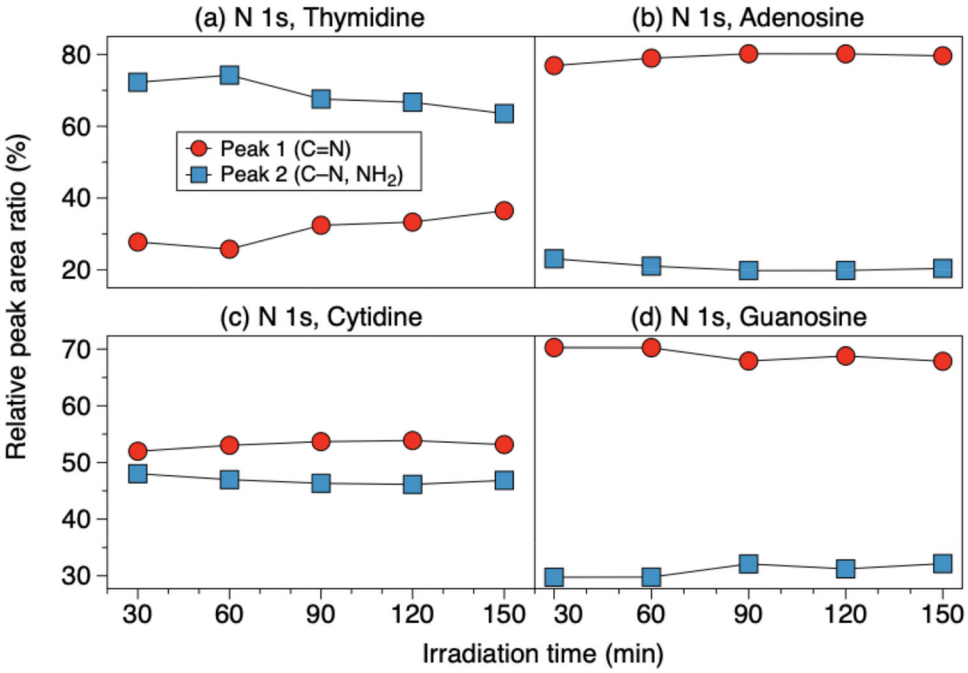

Fig. 7 Relative N 1s peak area ratios of (**a**) thymidine, (**b**) adenosine, (**c**) cytidine, and (**d**) guanosine under 25 eV LEE irradiation for 30, 60, 90, 120, and 150 min

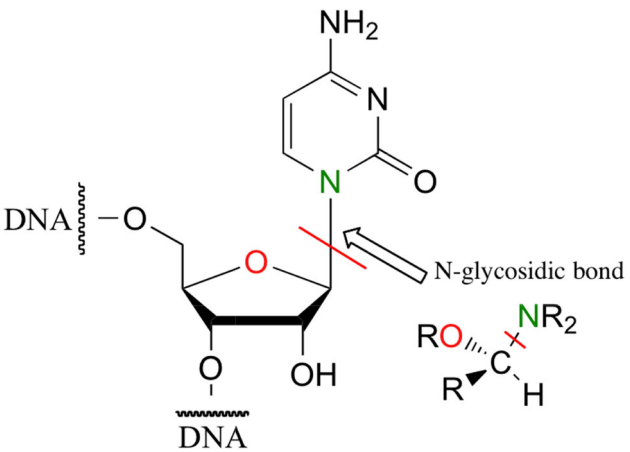

Fig. 8 Schematic representation of the N-glycosidic bond between deoxyribose and the nucleobase (cytosine shown as an example). The red line indicates the susceptible cleavage site under LEE irradiation, leading to base loss and formation of abasic sites

suggest the possible release of NH_2 groups and additional bond cleavages within the nucleobase. Notably, among the four nucleobases, only guanine exhibited a slight but measurable decrease in signal intensity during irradiation, suggesting that structural damage may be localized in both the base moiety and the N-glycosidic bond.

Figure 8 illustrates the cleavage of the N-glycosidic bond in DNA, which exists as a C–N single bond between the sugar and the nucleobase. Several studies involving electron bombardment of short single-stranded DNA fragments (e.g., GCAT) have reported the release of nucleobases upon irradiation [22]. The previous observations suggest that core-excited resonances formed by electron attachment to the bases can retain the excess electron long enough to induce dissociation of the N-glycosidic bond.

3.4 Structural changes in the DNA backbone revealed by the phosphorus signal

Phosphate exists exclusively in the backbone structure of DNA, where it forms phosphoester bonds that link the sugar moieties and give rise to the phosphodiester linkage. Thus, any changes in the phosphate signal indicate structural alterations in the DNA backbone. In our study, phosphate was present only in calf thymus DNA and was absent in the nucleosides and nucleobases. In the P 2p region (Fig. 2), a decrease in peak intensity accompanied by an increase in FWHM was observed, suggesting partial bond cleavage or the formation of multiple phosphorus-containing species with slightly different chemical environments. This phenomenon may result from cleavage of the phosphoester bond between the sugar and phosphate groups, forming fragments with lower phosphorus oxidation states. Surface reconstruction during irradiation may also expose more phosphorus sites, slightly enhancing some P 2p subpeak signals. A previous study suggested that the generation of oxygen anions (O^-) originates from the fragmentation of the phosphate group in the DNA backbone, specifically through cleavage of the O=P bond, rather than from the C=O groups present in thymine, guanosine, or cytosine [38].

Table 2 Relative elemental intensity ratios of carbon, oxygen, nitrogen, and phosphorus in calf thymus DNA as a function of irradiation time

	Elemental intensity ratio (%)			
Irradiation Time (min)	C	O	N	P
30	52.80	25.82	15.68	5.70
60	52.99	25.63	15.66	5.72
90	53.56	25.36	15.31	5.76
120	53.77	25.12	15.29	5.82

3.5 Overall changes for the elements

Significant damage, such as the release of hydroxyl groups (C–OH), cleavage of C–N bonds, and fragmentation of the DNA backbone, may alter the relative elemental composition of the samples. Table 2 presents the relative intensity ratios of carbon, oxygen, nitrogen, and phosphorus in calf thymus DNA as a function of irradiation time. Only minor variations ($< 1\%$) were observed, which fall within the estimated 10–20% uncertainty of XPS measurements, and therefore should be regarded as indicative rather than quantitative changes. Compared to the 30-min irradiation, after 120 min of exposure, the oxygen and nitrogen signals appeared slightly decreased, while those of phosphorus and carbon appeared slightly increased. The decrease in the O 1 s signal is consistent with possible loss of hydroxyl groups, whereas the decline in nitrogen may reflect C–N bond cleavage and subsequent release of nitrogen-containing fragments. The increased carbon signal could also be just a relative effect, driven by the decrease of other elemental signals. Phosphate-containing fragments may have been retained on the sample surface. A similar trend was observed for the P 2p signal, although the peak intensity decreased (Fig. 2), the relative phosphorus ratio increased after normalization because the O and N signals decreased more markedly.

4 Conclusions

In this study, XPS was employed to investigate structural changes in calf thymus DNA and its components after irradiation with 25 eV electrons. Spectral analysis of multiple core levels (O 1 s, C 1 s, N 1 s, and P 2p) showed that LEE exposure can induce specific chemical modifications in DNA molecules.

A decrease in signals associated with C–OH groups, particularly in the O 1 s and C 1 s spectra, is consistent with possible detachment of hydroxyl groups from the sugar moiety. Changes observed in the C–N components of both the C 1 s and N 1 s regions suggest cleavage of the N-glycosidic bond. Broadening and weakening of the P 2p signals may indicate damage to the phosphate backbone in calf thymus DNA. These changes indicate progressive molecular fragmentation along with changes in elemental composition. With longer irradiation, oxygen and nitrogen signals gradually decreased, while the relative intensities of carbon and phosphorus slightly increased.

Different nucleosides and their specific structural sites exhibited varying responses to LEE irradiation. Similar to the observations in calf thymus DNA, thymidine and guanosine showed more pronounced spectral changes, whereas cytidine and adenosine remained relatively stable. Compared to their corresponding nucleobases, nucleosides were more susceptible to modification by LEE exposure. Nevertheless, due to signal overlap and limited spectral resolution, structural interpretation requires careful consideration.

This work provides experimental evidence of site-selective and base-specific damage caused by low-energy electrons. It offers insight into electron-induced molecular fragmentation in DNA systems and supports further development of precision strategies in radiation-based therapies.

Acknowledgements J.P.d.S. acknowledges support from the Portuguese National Funding Agency FCT-MCTES through Grant PD/BD/142768/2018, under the Radiation Biology and Biophysics Doctoral Training Programme (RaBBiT, PD/00193/2012), as well as a Fulbright Foundation grant. F.F.d.S. and J.P.d.S. further acknowledge support from FCT through Research Grant UID/FIS/00068/2020. H.Y., B.C., P.S., and S.P. acknowledge support from the U.S. Department of Energy, Office of Science, Office of Basic Energy Sciences, under Award No. DE-FC02-04ER15533. This is contribution number NDRL 5473 from the Notre Dame Radiation Laboratory.

Author contributions

Conceptualization: Sylwia Ptasińska. Investigation: João Pereira-da-Silva, Bo-An Chen, Pitambar Sapkota. Data Curation: João Pereira-da-Silva, Hao Yu. Formal Analysis: Hao Yu. Visualization: Hao Yu, João Pereira-da-Silva. Writing—Original Draft: João Pereira-da-Silva, Hao Yu. Writing—Review and Editing: João Pereira-da-Silva, Hao Yu, Bo-An Chen, Pitambar Sapkota, Filipe Ferreira da Silva, Sylwia Ptasińska. Supervision: Filipe Ferreira da Silva, Sylwia Ptasińska.

Data availability All data supporting the findings of this study are available within the article and its supplementary materials, and additional data are available from the authors upon reasonable request.

References

1. M. Ahmad, L.T. Jung, A.-A. Bhuiyan, From DNA to protein: why genetic code context of nucleotides for DNA signal processing? A review. Biomed. Signal Process. Control **34**, 44–63 (2017)
2. A. Wada, A. Suyama, Local stability of DNA and RNA secondary structure and its relation to biological functions. Prog. Biophys. Mol. Biol. **47**(2), 113–157 (1986)
3. P. Jeggo, M. Löbrich, DNA double-strand breaks: their cellular and clinical impact? Oncogene (2007). https://doi.org/10.1038/sj.onc.1210868
4. M.A. Huels, B. Boudaïffa, P. Cloutier, D. Hunting, L. Sanche, Single, double, and multiple double strand breaks induced in DNA by 3–100 eV electrons. J. Am. Chem. Soc. **125**(15), 4467–4477 (2003)
5. L. Sanche, Interaction of low energy electrons with DNA: applications to cancer radiation therapy. Radiat. Phys. Chem. **128**, 36–43 (2016)
6. E.J. Hall, A.J. Giaccia, *Radiobiology for the Radiologist* (Lippincott Williams & Wilkins, Philadelphia, 2006)
7. A. Kumar, D. Becker, A. Adhikary, M.D. Sevilla, Reaction of electrons with DNA: radiation damage to radiosensitization. Int. J. Mol. Sci. **20**(16), 3998 (2019)
8. R. Barrios, P. Skurski, J. Simons, Mechanism for damage to DNA by low-energy electrons. J. Phys. Chem. B **106**(33), 7991–7994 (2002)
9. I. Baccarelli, I. Bald, F.A. Gianturco, E. Illenberger, J. Kopyra, Electron-induced damage of DNA and its components: experiments and theoretical models. Phys. Rep. **508**(1–2), 1–44 (2011)
10. S. Ptasińska, A. Stypczyńska, T. Nixon, N.J. Mason, D.V. Klyachko, L. Sanche, X-ray induced damage in DNA monitored by X-ray photoelectron spectroscopy. J. Chem. Phys. (2008). https://doi.org/10.1063/1.2961027
11. M. McAllister, M. Smyth, B. Gu, G.A. Tribello, J. Kohanoff, Understanding the interaction between low-energy electrons and DNA nucleotides in aqueous solution. J. Phys. Chem. Lett. **6**(15), 3091–3097 (2015)
12. P. O'Neill, E. M. Fielden, Primary free radical processes in DNA. In *Advances in radiation biology*, vol. 17 (Elsevier, 1993), p 53–120
13. R. Roots, S. Okada, Estimation of life times and diffusion distances of radicals involved in x-ray-induced DNA strand breaks of killing of mammalian cells. Radiat. Res. **64**(2), 306–320 (1975)
14. H. Yu, S. Yamashita, Radical scavenging and chemical repair of rutin observed by pulse radiolysis: as a basis for radiation protection. Free Radic. Res. **53**(9–10), 1005–1013 (2019)
15. M.B. Hahn, P.M. Dietrich, J. Radnik, In situ monitoring of the influence of water on DNA radiation damage by near-ambient pressure X-ray photoelectron spectroscopy. Commun. Chem. **4**(1), 50 (2021)
16. B. Boudaıffa, P. Cloutier, D. Hunting, M.A. Huels, L. Sanche, Resonant formation of DNA strand breaks by low-energy (3–20 eV) electrons. Science **287**(5458), 1658–1660 (2000)
17. E. Alizadeh, T.M. Orlando, L. Sanche, Biomolecular damage induced by ionizing radiation: the direct and indirect effects of low-energy electrons on DNA. Annu. Rev. Phys. Chem. **66**(1), 379–398 (2015)
18. Y. Gao, Y. Zheng, L. Sanche, Low-energy electron damage to condensed-phase DNA and its constituents. Int. J. Mol. Sci. **22**(15), 7879 (2021)
19. B. Boudaïffa, P. Cloutier, D. Hunting, M. Huels, L. Sanche, Cross sections for low-energy (10–50 eV) electron damage to DNA. Radiat. Res. **157**(3), 227–234 (2002)
20. H. Abdoul-Carime, P. Cloutier, L. Sanche, Low-energy (5–40 eV) electron-stimulated desorption of anions from physisorbed DNA bases. Radiat. Res. **155**(4), 625–633 (2001)
21. X. Pan, L. Sanche, Dissociative electron attachment to DNA basic constituents: the phosphate group. Chem. Phys. Lett. **421**(4–6), 404–408 (2006)
22. Y. Zheng, P. Cloutier, D.J. Hunting, J.R. Wagner, L. Sanche, Phosphodiester and N-glycosidic bond cleavage in DNA induced by 4–15 eV electrons. J. Chem. Phys. (2006). https://doi.org/10.1063/1.2166364
23. H. Abdoul-Carime, S. Gohlke, E. Fischbach, J. Scheike, E. Illenberger, Thymine excision from DNA by subexcitation electrons. Chem. Phys. Lett. **387**(4–6), 267–270 (2004)
24. S. Ptasińska, P. Candori, S. Denifl, S. Yoon, V. Grill, P. Scheier, T. Märk, Dissociative ionization of the nucleosides thymidine and uridine by electron impact. Chem. Phys. Lett. **409**(4–6), 270–276 (2005)
25. H. Abdoul-Carime, J. Langer, M. Huels, E. Illenberger, Decomposition of purine nucleobases by very low energy electrons. European Phys. J. D-Atomic. Mol. Opt. Plasma. Phys. **35**, 399–404 (2005)
26. D. Huber, M. Beikircher, S. Denifl, F. Zappa, S. Matejcik, A. Bacher, V. Grill, T. Märk, P. Scheier, High resolution dissociative electron attachment to gas phase adenine. J. Chem. Phys. (2006). https://doi.org/10.1063/1.2336775
27. H.-A. Noh, H. Cho, XPS study on DNA damage by low-energy electron irradiation. J. Radiat. Prot. Res. **36**(4), 190–194 (2011)
28. H.-A. Noh, Y.-S. Park, H. Cho, XPS study on the effect of low-energy electron irradiation on DNA damage by Fe 3+ ion. J. Radiat. Prot. Res. **40**(2), 87–91 (2015)
29. X. Zhang, S. Ptasinska, Dissociative adsorption of water on an H_2O/GaAs (100) interface: in situ near-ambient pressure XPS studies. J. Phys. Chem. C **118**(8), 4259–4266 (2014)

30. S. M. Tougaard, Validity of automated x-ray photoelectron spectroscopy algorithm to determine the amount of substance and the depth distribution of atoms. J. Vac. Sci. Technol. A **31**, 031503 (2013). https://doi.org/10.1116/1.4795246
31. M. Ramstedt, A. Shchukarev, XPS spectra from nucleobases, DNA, and RNA. Surf. Sci. Spectra (2023). https://doi.org/10.1116/6.0002368
32. X. Pan, L. Sanche, Mechanism and site of attack for direct damage to DNA by low-energy electrons. Phys. Rev. Lett. **94**(19), 198104 (2005)
33. S. Kawanishi, Y. Hiraku, S. Oikawa, Mechanism of guanine-specific DNA damage by oxidative stress and its role in carcinogenesis and aging. Mutat. Resear/Rev. Mutat Resear **488**(1), 65–76 (2001)
34. J. Cadet, T. Douki, D. Gasparutto, J.-L. Ravanat, Oxidative damage to DNA: formation, measurement and biochemical features. Mutat. Resear/Fundam. Mol. Mech. Mutagen. **531**(1–2), 5–23 (2003)
35. S. Steenken, S.V. Jovanovic, How easily oxidizable is DNA? One-electron reduction potentials of adenosine and guanosine radicals in aqueous solution. J. Am. Chem. Soc. **119**(3), 617–618 (1997)
36. N. Mirsaleh-Kohan, A.D. Bass, P. Cloutier, S. Massey, L. Sanche, Low energy electron stimulated desorption from DNA films dosed with oxygen. J. Chem. Phys. (2012). https://doi.org/10.1063/1.4729781
37. A.C. Drohat, A. Maiti, Mechanisms for enzymatic cleavage of the N-glycosidic bond in DNA. Org. Biomol. Chem. **12**(42), 8367–8378 (2014)
38. X. Pan, P. Cloutier, D. Hunting, L. Sanche, Dissociative electron attachment to DNA. Phys. Rev. Lett. **90**(20), 208102 (2003)